The stromal side of the cytochrome b6f complex regulates state transitions

Alexis Riché, Louis Dumas, Soazig Malesinski, Guillaume Bossan, Céline Madigou, Francesca Zito, Jean Alric

The stromal side of cytochrome b_6f complex regulates state transitions

Alexis Riché[1], Louis Dumas[1], Soazig Malesinski[1], Guillaume Bossan[2], Céline Madigou[2], Francesca Zito[2], Jean Alric[1]

Affiliations

[1] Institut de biosciences et biotechnologies d'Aix-Marseille, Unité Mixte de Recherche 7265, Commissariat à l'Énergie Atomique, Centre National de la Recherche Scientifique, Aix-Marseille Université, CEA Cadarache, Bâtiment 1900, 13108 Saint-Paul-lez-Durance, France

[2] Laboratoire de Biologie Physico-Chimique des Protéines Membranaires Unité Mixte de Recherche 7099, Université Paris Cité, Centre National de la Recherche Scientifique, Institut de Biologie Physico-Chimique, 13 rue Pierre et Marie Curie F-75005 Paris, France

Corresponding author

Jean Alric jean.alric@cea.fr

Classification

Biological Sciences, Plant Biology

Keywords

Cytochrome b_6f complex, photosynthetic electron transport, regulation, phosphorylation, protein kinase

The author responsible for distribution of materials integral to the findings presented in this article in accordance with the policy described in the Instructions for Authors (https://academic.oup.com/plcell/pages/General-Instructions) is: Jean Alric (jean.alric@cea.fr).

Abstract

In oxygenic photosynthesis, state transitions distribute light energy between Photosystem I and Photosystem II. This regulation involves the reduction of the plastoquinone pool, activation of the STT7 protein kinase by cytochrome b_6f complex, phosphorylation and migration of Light Harvesting Complexes II (LHCII). Here we show the C-term of cyt b_6 subunit acts on phosphorylation of STT7 and state transitions. We used site-directed mutagenesis of the chloroplast *petB* gene to truncate (remove L215^{b_6}) or elongate (add G216^{b_6}) the cyt b_6 subunit. Modified complexes are devoid of heme c_i and degraded by FTSH protease, revealing that salt bridge formation between cyt b_6 (PetB) and subunit IV (PetD) is key to the assembly of the complex. In double mutants where FTSH is inactivated, modified cyt b_6f are accumulated but the phosphorylation cascade is blocked. We also replaced the arginine interacting with heme c_i propionate (*R207K*^{b_6}). In this modified complex, heme c_i is present but the kinetics of phosphorylation are slower. We show that highly phosphorylated forms of STT7 are accumulated transiently after reduction of the PQ pool, and represent the active forms of the protein kinase. Phosphorylation of the LHCII targets is favored at the expense of the protein kinase, and the migration of LHCII towards PSI is the limiting step for state transitions.

Significance statement

State transitions are regulatory mechanisms that optimize the quantum yield of photosynthesis. *Chlamydomonas reinhardtii* is the choice organism to study this regulation at the molecular level. Our study describes an unprecedented mechanism of stereochemical changes at the Q_i site of the cytochrome b_6f complex that trigger STT7 protein kinase activation through autophosphorylation.

Abbreviations

Cyt, cytochrome; stt, state transitions; suIV, subunit IV

Introduction

In oxygenic photosynthesis, two photosystems PSII and PSI, connected by the cytochrome b_6f complex, work in series to transfer electrons from a primary electron donor, water, to a terminal electron acceptor, $NADP^+$. Electron transfer is coupled to proton translocation across the thylakoid membrane for generating a proton-motive force used for ATP synthesis. The reduction of CO_2 into C3 compounds requires ATP and NADPH. State transitions optimize the yield of photosynthesis by distributing the mobile light harvesting complexes II (LHCII) between PSII and PSI. When the plastoquinone (PQ) pool is oxidized, dephosphorylated LHCII attach to PSII (State 1), and conversely when the excitation pressure on PSII is high, giving an reduced PQ pool, LHCII are phosphorylated and migrate towards PSI (State 2) [1]. In *Chlamydomonas reinhardtii* the STT7 protein kinase contains a transmembrane helix and a stromal kinase domain that phosphorylates LHCII [2]. The PBCP and PPH1 phosphatases, localized to the stroma of chloroplasts, dephosphorylate LHCII [3]. Whereas PBCP and PPH1 are constitutively active, STT7 activity is regulated by a number of factors; in the absence of cytochrome b_6f complex [4], or when its lumenal PQ binding site Q_o is obstructed [5–7], state transitions are blocked. The transmembrane domain of STT7 interacts with cytochrome *f* and the Rieske subunit of cyt b_6f [8,9]. The kinase domain of STT7 is on the other side of the thylakoid membrane where the stromal loop of cyt b_6f subunit IV, between helixes F and G, allows for STT7 autophosphorylation *in vitro* [10].

In mitochondrial and bacterial cytochrome bc_1, the cytochrome *b* subunit contains 8 transmembrane helixes and it is encoded by a single *petB* gene, see Figure 1A. In cyanobacteria and chloroplasts, cytochrome b_6f complex binds a chlorophyll a and a β-carotene molecule, and the cytochrome *b* is split in cyt b_6 and subunit IV (suIV), see Figure 1B, encoded by *petB* and *petD* respectively. While the split of cytochrome *b* into b_6 and suIV leaves the coordination of the *b*-hemes and the quinone binding pocket Q_o unchanged [11], several structural rearrangements take place: helix H is lost and heme c_i occupies the Q_i site, covalently bound by $C35^{b_6}$. Because of these structural differences to the cyt bc_1 complex, the stromal side of the cyt b_6f complex is a good example of how distinct evolutionary features were maintained in respiratory *vs.* photosynthetic membranes. In addition, modified cyt b_6f complexes are prone to degradation by the nuclear-encoded thylakoid ATP-dependent zinc metalloprotease FTSH[12]. FTSH from *Chlamydomonas reinhardtii* comprises two subunits, FTSH1 and FTSH2. In this work, we made use of an available mutation in *FTSH1*[12] to restore photosynthesis in mutants where cyt b_6f accumulation was impaired.

In a previous work [10] we noted that the C-terminal end of the cytochrome b_6 subunit forms a salt bridge with Arg125 of suIV. We showed R125^{suIV} is involved in a direct interaction with the STT7 protein kinase. Truncation or elongation of cyt b_6 was done by removing the last Leu215 (*xL215*^{b_6}) or adding an extra Gly216 (*G216*^{b_6}). Amino acid R207^{b_6}, that interacts with the propionate group of heme c_i in cytochrome b_6f crystal structure [11], was substituted with a similarly positively charged Lys in strain *R207K* ^{b_6}.

In this work we confirmed that the stromal region of cyt b_6f is intimately connected to the STT7 protein kinase, not only at the level of suIV, but also through an interaction with the C-terminal part of cyt b_6. In a variety of strains, we studied the kinetics of state transitions using a variety of techniques and protein phosphorylation using PhosTag PAGE and western blot to propose a mechanistic model for state transition.

Results

Truncated or elongated versions of cyt b_6 are degraded by FTSH

C. reinhardtii mutants were obtained by site-directed mutagenesis and chloroplast transformation of a *ΔpetB* strain with pWBA plasmids carrying an *aadA* resistance cassette and various mutated versions of the *petB* gene (for the complete list of strains used in this study see Supplementary Table S1). Transformants were selected on TAP medium supplemented with spectinomycin and sequenced to verify the presence of the mutated *petB* genes. While we successfully complemented two different *ΔpetB* strains with the pWBA plasmid carrying the WT *petB* gene, the mutants (*R207K*, *xL215* and *G216*) did not accumulate the cyt b_6 subunit (Supplementary Figure S1) neither did they grow under photoautotrophic conditions. Therefore, cyt b_6 C-terminal modifications specifically impede cyt b_6f assembly and function.

The mutant with an inactivated FTSH protease [12] (R420C substitution in strain *ftsh1-1*, kindly provided by Catherine de Vitry) was then used as a host strain for transformation with the pWBA plasmids carrying mutated or non-mutated *petB*. Transformants were selected on TAP medium containing spectinomycin. Genotyping by PCR showed homoplasmy was reached after > 3 months of restreaking under antibiotic resistance pressure, see Supplementary Figure S2.

Genetically modified strains were tested on plates and compared to reference strains (Figure 2). WT and *stt7-1* [2] grew on tris-acetate-phosphate (TAP) and minimal (MIN) media while the cyt b_6f-less strain *ΔpetB* [13] required acetate. The control strain (*ftsh1-1* transformed with non-

mutated pWBA plasmid*) ftsh*, and site-directed mutants of the *petB* gene *R207K*^{b6}, *xL215*^{b6} and *G216*^{b6} were able to grow slowly under phototrophic conditions. Mutants *xL215*^{b6} and *G216*^{b6} have low photosystem II quantum yield ϕ_{PSII} and high F_M'/F_M (see Materials and Methods for chlorophyll fluorescence), similarly to *ΔpetB*, while *ftsh* and *R207K*^{b6} showed little difference to the WT. The high fluorescence state of *xL215*^{b6} and *G216*^{b6} suggested they were blocked in State 1 whereas *R207K*^{b6} showed a decreased F_M' upon dark anaerobic adaptation, *i.e.* transited to State 2 in response to the reduction of the PQ pool (see Supplementary Figure S3 for the kinetics of F_M' decrease corresponding to the false color images of Figure 2). All strains had a similar F_V/F_M, showing the maximal quantum yield of PSII was not affected. F_V/F_M was even larger for mutants *stt7-1*, *xL215*^{b6} and *G216*^{b6}, consistently with being constitutively locked in State 1 (See also Supplementary Figure S3).

The increase of PSI antenna size in State 2 was detected using chlorophyll fluorescence emission spectra at 77K (see Supplementary Figure S4). State 2 was observed for the WT, *ftsh* and *R207K*^{b6} but absent in *stt7-1*, *xL215*^{b6} and *G216*^{b6} supporting a block of state transitions in these strains.

Truncated or elongated versions of cyt *b*$_6$ have a blocked Q-cycle

Cytochrome *b*$_6$*f* complex turnover (Q-cycle) was measured *in vivo* using flash-induced absorbance changes: electrochromic shift (ECS) and cyt *b* and *f* oxidation-reduction kinetics (see Figure 3). These measurements showed that cyt *b*$_6$*f* complexes accumulated to the same level as *ftsh* in *R207K*^{b6}, *xL215*^{b6} and *G216*^{b6}. Although the Q-cycle of *R207K*^{b6} was not affected, *xL215*^{b6} and *G216*^{b6} were blocked in the plastoquinone reduction site Q_i. The differences in cyt *f* reduction kinetics were not statistically relevant (overlapping 95%-confidence envelopes, half-time ranging from ~ 2.5 ms to ~ 10 ms). A difference of statistical significance was found only for cyt *b* oxidation kinetics between *ftsh* ($7.1 < t_{1/2} < 9.5$ ms) and *R207K*^{b6} ($12.2 < t_{1/2} < 15.6$ ms) and the two other mutants *xL215*^{b6} and *G216*^{b6} ($t_{1/2} > 100$ ms). Although the difference in cyt *b* reoxidation rates between *R207K*^{b6} and *ftsh* was statistically significant (Figure 3C), it did not affect the overall electron transport in the chain (see ϕ_{PSII} in Figure 2). In contrast, in the latter two mutants *xL215*^{b6} and *G216*^{b6}, electrogenic transport (Q-cycle in Figure 3D) and heme *b* reoxidation (Figure 3F) are impaired, showing a block of the low-potential chain at Q_i, and translating into a low photosystem II quantum yield ϕ_{PSII} in the light (Figure 2).

Truncation or elongation of cyt *b*$_6$ impedes the binding of heme *c*$_i$

158 Accumulation of various protein subunits were detected by total protein extraction from a
159 culture grown in TAP in low light (5-10 $\mu mol_{photons}\ m^{-2}\ s^{-1}$), SDS-PAGE and immunodetection
160 using specific antibodies (Figure 4). While *ΔpetB* , was devoid of cytochrome b_6 subunit [13], and
161 *stt7-1* lacked the STT7 kinase (Figure 4A), *ftsh* and $R207K^{b6}$ accumulated these proteins to WT
162 levels. $xL215^{b6}$ and $G216^{b6}$ mutants also accumulated normal levels of STT7 and cyt b_6.
163 Truncated cyt b_6 ($xL215^{b6}$) ran slightly faster on the gel than the elongated form ($G216^{b6}$) but
164 for both, the bands were much less diffuse than in all other samples (Figure 4C). Similar
165 changes in polypeptide mobility were reported for mutants affected for heme binding [14]. Heme
166 staining (TMBZ, tetramethylbenzamidine peroxidase activity) showed absence of cyt b_6 and a
167 90 % reduction of cyt *f* in *ΔpetB* while cyt *f* was detected in all other strains (Figure 4D). Only
168 $xL215^{b6}$ and $G216^{b6}$ showed absence of heme staining even though the b_6 polypeptide was
169 detected (Figure 4D). Our conclusion is that heme c_i does not bind covalently to the truncated
170 or elongated versions of the cyt b_6 subunit, and that modified complexes accumulate when
171 FTSH is inactivated.
172 *stt7-9* accumulated less of a higher molecular version of STT7, as previously reported [15] and
173 attributed to the expression of a putative STT7-Arg fusion. PETO (also referred as suV) is a
174 subunit loosely bound to cyt b_6f complex [16,17]. PETO was expectedly reduced in *ΔpetB* and
175 *iniD1-4* [18], a strain attenuated for cyt b_6f complex. *DLSΔ* [19], a *petD-petL* chimeric construct
176 assembling a suIV-PetL protein fusion, and $R125E^{suIV}$ [10] lost PETO as well (see Figure 4B),
177 although they accumulated WT amounts of the complex. It suggested a loss of interaction of
178 PETO with these modified suIV, and protein degradation. Different levels of PETO were also
179 observed in *ftsh*, $R207K^{b6}$, $xL215^{b6}$ and $G216^{b6}$, potentially supporting the destabilization of
180 protein-protein interactions at the cyt b_6 – suIV interface.
181

182 **STT7 phosphorylation in response to reducing conditions**

183 STT7 phosphorylation state was analyzed by polypeptide separation on PhosTag-SDS-PAGE
184 and immunodetection with STT7 antisera. Oxidizing conditions (ox) favoring State 1 were
185 obtained after 1 hour preillumination in the presence of DCMU under oxic conditions (rotary
186 shaken in air); and reducing conditions (red) were reached 10 min after addition of 5 µM FCCP
187 (membrane uncoupler) in the dark, boosting the glycolytic flux and the overflow of reductant.
188 Sampling of the proteins was done by fast quenching of cultures in cold acetone. When Phos-
189 Tag is incorporated to denaturing gels, the dephosphorylated polypeptide runs faster than the
190 phosphorylated polypeptide. Here in Figure 5, we denoted D–, P–, and PP– the three

phosphorylation forms recognized by the STT7-antiserum. In *stt7-1*, used as a negative control, neither in oxidizing nor in reducing conditions could we detect non-specific bands (see the two rightmost lanes in Figure 5A). In all other strains placed in oxidizing conditions, STT7 was detected as a major band, suggesting that the protein kinase accumulated mostly under its (D–) dephosphorylated form. After the WT was shifted to reducing conditions, this band disappeared, the migration of STT7 was significantly delayed and split into (P–) phosphorylated and (PP–) highly phosphorylated forms. The heterogeneity in STT7 phosphorylation levels was always, within experimental accuracy (see next section), in favor of the highly (PP–) phosphorylated forms (for example compare 5A, 5B and 5C). In the *DLSΔ* mutant, in which *petD* fusion to *petL* gives an extra helix to suIV, destabilizes STT7 binding and blocks state transitions [19], P– is accumulated at the expense of PP–. Similarly, in *iniD1-4*, attenuated in cyt b_6f complex [18], P– dominates over PP–. In cyt b_6f -less mutant *ΔpetB*, only P– is found, as it is in mutants accumulating cyt b_6f to WT levels, but blocked for state transitions (*PWYE*, $R125E^{suIV}$, $xL215^{b6}$, $G216^{b6}$). *ftsh* and $R207K^{b6}$ showed a distribution of STT7 between the three D–, P– and PP– forms with less immunoreaction. This attenuation of bands in PhosTag-PAGE was inconsistent with the similar levels of STT7 detected in Figure 4C. Therefore, we decided to address the time-dependence of the phosphorylation pattern.

Kinetics of STT7 phosphorylation and state transition

As in the experiments described above, cells were treated with DCMU and incubated for 1 h under light-oxic conditions (ox). At time $t = 0$ these cultures were transferred to the dark, and reducing conditions (red) were induced by addition of 5 µM of the membrane uncoupler FCCP (Figure 6). Proteins were sampled by fast quenching in cold acetone at various delays after the induction. Protein samples were loaded on PhosTag-PAGE and reacted against STT7 antiserum or on standard PAGE and immunoblotted with an anti-phosphothreonin (α-^{P}T) antibody.

In the WT (Figure 6A), in response to reducing conditions, and within the time-resolution of the sampling (2-5 min) the D–form of STT7 disappeared and the PP–form accumulated. At the same time, LHC2 polypeptides P13 (LHCBM3,4,6,8,9) and P17 (LHCBM2) [20,21] were substantially increased in their phosphorylation states. At $t \geq 10$ min, the PP–form steadily decreased while the P–form increased. However, P13/P17 stayed phosphorylated during the course of the kinetics.

In *ftsh* (Figure 6B), PP−formation was delayed, showing a maximal accumulation at $5 \leq t \leq 15$ min. Phosphorylation of P13/P17 peaked at t = 15min. In *R207K*^{b_6} (Figure 6C), PP−formation was further delayed to $10 \leq t \leq 20$ min while the P−form was still detected in a non-negligible amount. P13/P17 phosphorylation peaked at t = 30 min. At $t \geq 30$ min, PP− and P−form were destabilized in both *ftsh* and *R207K*^{b_6}, and STT7 returned to its D−form. In a kinetics model of competing chemical reactions, the reaction rates and the level of accumulation of reaction intermediates are linked, slower phosphorylation rates of STT7 are consistent with less phosphorylated state of STT7 at t = 0 .

Discussion

The C-term of cyt b_6 straps the complex subunits together

The chloroplast cytochrome b_6f complex is involved in photosynthetic electron transport while its mitochondrial counterpart, the cytochrome bc_1 complex is involved in respiration. Apart from the difference between cyt c_1 and cyt *f*, which play very similar roles in terms of electron transport, the most significant genetic difference is that the bacterial and mitochondrial *petB* gene is split into *petB* and *petD* in chloroplast or cyanobacterial version of the *b*-type cytochrome [22]. The *petB-petD* split co-occurs with the presence of C35^{b_6}, forming the thioether bond to the c_i heme. Therefore, the fragmentation of the core subunits of the complex was thought [11] to accommodate heme c_i insertion [23]. Here we show that the truncation (*xL215*^{b_6}) or elongation (*G216*^{b_6}) of the cyt b_6 do not allow for cyt b_6f accumulation, neither does the modification of the vicinity of heme c_i's propionate (*R207K*^{b_6}), this could involve a general quality control of the complexes by the FTSH protease. Accordingly, since heme c_i does not bind covalently to C35^{b_6} in the presence of a modified C-term of cyt b_6, cyt b_6f accumulation is only favored when FTSH is inactivated. We therefore conclude that the salt-bridge formed between the C-term of cyt b_6 and suIV straps these two subunits together. When loosened (*G216*^{b_6}) or fastened (*xL215*^{b_6}), the strap fails to stabilize the CCB2-4/CCB3/cyt b_6 transient heme c_i ligation complex [24]. The final step of assembly of the complex being aborted (*G216*^{b_6}, *xL215*^{b_6}) or altered (*R207K*^{b_6}) modified complexes are degraded by FTSH.

The Q-cycle is required for efficient electron transport at steady state

The *G216*^{b6} and *xL215*^{b6} mutant cells showed slower photoautotrophic growth than the WT or *ftsh* strains. This is reminiscent of the *QiKO* strain [25], where the cyt b_6f complex lacks both hemes c_i and b_H. Malnoë and coworkers showed although the single turnover of the Q_o site was unchanged, the multi-turnover rate of the complex was 5% of the WT, this residual flux being attributed to a back-reaction from reduced heme b_L to the semiquinone in Q_o. In our work on the *G216*^{b6} and *xL215*^{b6} mutants lacking only c_i, we confirmed that quinol oxidation at the Q_o site was not affected: flash-induced bifurcated electron transfer from Q_oH_2 to heme *b* and *f* was unchanged. In contrast, the steady-state electron transport, requiring multi-turnover of the complex via the Q-cycle, was impaired at the step of quinone reduction at Q_i. This is due to the absence of heme c_i, a cofactor missing in the electron-transport chain, and a modified protein moiety in the quinone binding site. As noted previously, F40^{suIV} shapes the cavity and gates the quinone access to the heme iron [26,27]. The *F40Y*^{suIV} mutant shows a slower heme *b* re-oxidation during single-turnover reactions but is lacking a phenotype in multiple-turnover settings[26]. Another hint about heme c_i in the Q_i catalysis comes from the *R207K*^{b6} mutant, where R207 ^{b6}, interacting with heme c_i propionate, was replaced by a K. In *R207K*^{b6}, cyt *b* reoxidation rate was 60% slower (statistically significant). Although it may be relevant for the function of the Q_i site, it did not have any significant effect on the overall electron transport rate nor on the photosynthetic growth rate of the cells.

The stromal side of the cyt b_6f complex is a protein docking site for STT7, PETO and other proteins

For the functional study of the modified cyt b_6f complexes, we used *ftsh1-1* as a host for the genetic engineering [25]. We found in *G216*^{b6} and *xL215*^{b6}, that cyt b_6 subunit accumulated to WT levels, and retained PETO [4]. In contrast, PETO accumulation is reduced *DLSΔ* and *R125E*^{suIV}. We take this as a support to the crosslinking data and model of interaction between PETO and suIV [17], and suggest that unbound PETO gets degraded by proteases. Although PETO is phosphorylated in State 2 [16], the presence or absence of PETO does not have any influence on state transitions [28]. This algal-specific protein may rather stabilize cyt b_6f supercomplexes under anaerobic conditions [28]. In cyanobacteria, R125^{suIV} binds to PETP [29] instead of PETO or STT7 [10]. As for Chlamydomonas PETO, cyanobacterial PETP may regulate the dynamic interaction of cyt b_6f complex with other protein complexes [30]. In the spinach cyt b_6f complex, the thylakoid soluble phosphoprotein (TSP9) is docked to the cyt b_6 – suIV stromal interface [31]. The binding / release mechanism proposed below for STT7 may work similarly for PETP and TSP9, providing a regulatory control on the signaling or metabolic pathways involving PETP and TSP9.

A phosphorylation model for state transitions

In Figure 5A we showed a phosphorylation of STT7, from the dephosphorylated form D– to the mildly phosphorylated P–form, that occurred in the absence of the cytochrome b_6f complex. This is represented in Figure 7 as steps ① and ②, independent from cytochrome b_6f complex. However, it does not indicate that the STT7 P–form ② is required for binding to the cyt b_6f ③. Although not involved in the phosphorylation step from ① to ②, cyt b_6f may bind the D–form ① (see dotted line) as well as the P–form ② (solid line). Despite cyt b_6f being 20 times more abundant than the protein kinase [8], we showed here that a ~10-fold decrease in the amount of cyt b_6f becomes limiting for STT7 phosphorylation (see *iniD1-4* lane in Figure 5A). The STT7 protein kinase directly interacts with cytochrome b_6f complex suIV , which induces STT7 autophosphorylation when ATP is added [10]. This is represented in Figure 7 as central steps ③ to ④.

The activation of STT7 through the highly phosphorylated PP–form in step ④, is necessary for the phosphorylation of LHCII, represented here as step ⑥. In the WT strain, the full phosphorylation of LHCII is reached in less than 2 min of incubation under reducing conditions, *i.e.* much faster than the kinetics of state transitions. It shows that the limiting step for state transitions is not the phosphorylation of LHCII but the migration of LHCII from PSII to PSI. When the formation of the highly phosphorylated forms of STT7 ④ is slowed down, like in the *ftsh* mutants and the $R207K^{b_6}$ substitution mutant, the sampling of the reaction steps allows for a better time-resolution of the phosphorylation kinetics. Since the FTSH1/2 protease hexamer is still present in the *ftsh* genetic background (with inactive FTSH1-R420C) it should transiently colocalize, as part of the quality control on thylakoid proteins, with its potential substrates (such as native or $R207K^{b_6}$ cyt b_6f complex). Atypical dwelling due to FTSH1-R420C might interfere with STT7/ b_6f interaction and thus could slow down state transitions. In Figure 6C, the phosphorylation of the P13 polypeptide seems to occur before P17, and P13 remains phosphorylated to the detriment of P17, see step ⑦. P13 and P17 appear phosphorylated at the expense of the STT7 PP–form, which returns to the P– or to the D–forms, the latter being strongly favoured at 60 minutes in the $R207K^{b_6}$ mutant. It suggests the PBCP / PPH1 phosphatases have a lesser affinity for P13, step ⑧ to ⑨ (see Figure 6C).

At this stage, it is still unclear how many phosphorylation reactions occur in the transient STT7-LHCII complex at step ⑥. Activated STT7 PP–form may hydrolyse ATP to phosphorylate

several LHCII complexes. It is also possible that STT7 PP−form transfers a phosphate to LHCII and requires cyt b_6f reactivation to reset to the PP−form.

Role of the quinone binding sites Q_o and Q_i

In support to previous work [5,6], we confirm here that the quinone binding site Q_o plays a pivotal role in state transitions: Figure 5B shows that STT7 is blocked under its P−form in the PWYE mutant, blocked in the Q_o site. In accordance with STT7 being blocked in the P−form in the strain devoid of cyt b_6f complex, a functional Q_o site, and movement of the Rieske protein [7], may be required for the binding of cyt b_6f complex to STT7 through its transmembrane helix and luminal extension.

In the cyt b_6f complex crystal structure, the C-terminal carboxylate group of cyt b_6 interacts with the guanidinium group of $R125^{suIV}$ ⑤. *In vivo*, this salt-bridge can be broken to allow $R125^{suIV}$ to interact with STT7 ③ and ④ [10]. A similar protein-protein interaction is found in the α1α2β1β2 complex of deoxyhemoglobin: a salt bridge is formed between the C-terminal of the β1 subunit and the amino group of Lys40 in the α2 subunit. This bond is broken upon oxygen binding to the heme iron (oxyhemoglobin) [32]. This conformational change accounts for the cooperative binding of the other three oxygen molecules in the complex. In the cytochrome b_6f complex, the binding/release of ligands to the heme c_i iron may induce similar long-distance stereochemical changes. The Q_i site can accommodate quinone analogs such as the NQNO inhibitor or heme iron ligands like carbon monoxide (CO) [33–35]. Both chemicals change heme c_i's midpoint redox potential. Heme c_i titrates in two pH-dependent waves in the presence of NQNO, showing an equilibrium between two conformations of the complex [33]. Taken together, our results suggest that depending on Q_i occupancy and conformation of R207 ^{b_6} interacting with heme c_i propionate [36], the unpinning of cyt b_6-COOH from $R125^{suIV}$, is a signal for STT7 kinase activation *via* autophosphorylation.

Materials and Methods

***Chlamydomonas* strains and growth conditions**

The *Chlamydomonas reinhardtii* strains used in this study are listed in Table 1. They were maintained under photoheterotrophic conditions on Tris-acetate phosphate (TAP) plates supplemented with 2% agar at 25°C under 5-10 $\mu mol_{photons}\ m^{-2}\ s^{-1}$. Photoautorophic growth was tested in minimum (MIN) medium. Liquid cultures were grown in liquid TAP medium under the same light intensity unless indicated otherwise. Light was provided by "warm white" LEDs. WT t222 (IBPC, Paris), derivated from 137c [37], was used as a reference strain in this work.

Plasmids and *petB* mutants

Plasmid pWBA containing the *aadA* (spectinomycin-resistance) cassette [38] downstream of WT *petB* was used for mutagenesis and chloroplast transformation. When transformed in the *ΔpetB* strain, the site-directed mutated strains were noted *R207K, xL215*, and *G216* see Supplementary Figure S1. The *ftsh 1-1* strain [12] was then used as the host strain for chloroplast transformation. The control strain, *ftsh* (*ftsh 1-1* transformed with non-mutated pWBA plasmid) and site-directed mutated strains (note the b_6 superscript) $R207K^{b_6}$, $xL215^{b_6}$ (truncation of the cyt b_6 by deleting L215) and $G216^{b_6}$ (elongation of the cyt b_6 by adding a Gly at position 216) were obtained using mutated pWBA plasmids as follows. Plasmid DNA was precipitated on gold particles using the Seashell Technology S550d gold DNA protocol. *ftsh1-1* cells spread on TAP medium with 150 $\mu g.mL^{-1}$ spectinomycin were transformed by gold particle bombardment. After transformation, cells were left to recover in the dark for up to 24 h and transformants were incubated under low light (5-10 $\mu mol_{photons}\ m^{-2}\ s^{-1}$). Transformants were transferred repeatedly on TAP + spectinomycin medium until homoplasmy was reached.

Genotyping

DNA extraction was performed using the "Chelex" method. Clones were resuspended in 30 µL H_2O, 30 µL of ethanol was added and the mix was vortexed for 3s. 200 µL of 5 % Chelex 100 solution (Bio-Rad) was added before 8min incubation at 95 °C. Resin was pelleted by centrifugation and supernatant was used as template for PCR. Genotyping PCRs were performed using WT-specific primers for each mutation. Sensitivity and selectivity of the amplifications were checked using diluted WT DNA extract, see Supplementary Figure S2. Mutations were confirmed by sequencing of the target region of *petB*.

Chlorophyll fluorescence measurements

Chlorophyll fluorescence was measured on cells grown on plates using a laboratory built system [39]. Maximum quantum efficiency of PSII [$F_V / F_M = (F_M - F_0) / F_M$], PSII quantum yield [$\phi_{PSII}$

386 = (F_M – F) / F_M] under 500 $\mu mol_{photons}$ m^{-2} s^{-1}. PQ pool was oxidized by a 15min dark adaptation
387 before transfer to anaerobic conditions (N_2 flush) and F_M' / F_M was recorded during a 10 min
388 period in the dark with 200 ms saturating pulses.
389
390 **Time-resolved spectrophotometry**
391 Flash-induced absorbance changes were measured using a JTS10 spectrophotometer
392 (BioLogic) upgraded by Daniel Béal (JBeamBio) where the light source is a pulsed light-
393 emitting diode and the measuring wavelength is selected through various interference filters.
394 Single turnover sub-saturating flashes are provided by a pulsed Nd:YAG laser pumping an
395 optical parametric oscillator (Continuum lasers). For a guide of good practice using this
396 apparatus, see the recent work of Mathiot and Alric [40]. Treatment with 10 µM DCMU and 1 mM
397 hydroxylamine fully inhibited Photosytem II after a preillumination. The actinic flash instantly
398 oxidizes P700, then Plastocyanin (few microseconds), then cyt *f* (few hundreds of
399 microseconds) / Rieske Iron-Sulfur Protein, then the quinol (QH_2) bound in Q_o. Therefore, the
400 cyt *f* reduction phase (~3 ms at 554 nm) corresponds to quinol oxidation. The second electron
401 from the quinol is directed towards the low potential chain and transferred to heme b_L and heme
402 b_H. At room temperature, these hemes are very close in absorbance and barely distinguishable
403 [41]. In practice, after > 1 hour dark anaerobic adaptation, b_H becomes reduced, due to the
404 reducing poise inside the cells. Following a PSI flash excitation, the injection of an electron in
405 the low potential chain therefore reduces b_L, giving a small transient increase at 563 nm, while
406 both b_H and b_L are being oxidized by the quinone in Q_i, observable as a net decrease in
407 absorbance. After the flash, a long-lived oxidized *b* heme signal is taken as an internal control
408 that b_H was reduced prior to the flash. Repetitive flashes increase the reduction phase and
409 decrease the net oxidation, showing the randomization of the redox state of the *b* hemes through
410 multiple Q-cycles [42].

411 After centrifugation, cells were resuspended at similar cell density, estimated from colorimetric
412 assay. On samples treated with hydroxylamine and DCMU at 50 µs and 520 nm, flash-induced
413 absorbance changes were typically 5 +/- 1 mO.D. Kinetics of the various strains were
414 normalized to 1 at 50 µs and 520 nm (see Figure S5A). The same normalization factor was
415 applied to cyt *f* and cyt *b*. Cyt *f* (554 nm) and cyt *b* (563 nm) oxidation-reduction kinetics were
416 extracted from ECS contribution using the built-in deconvolution procedure drawing a straight
417 baseline from 546 nm to 573 nm, as:

$$\text{cyt } f = \Delta A_{554\text{ nm}} - \Delta A_{573\text{ nm}} - (\Delta A_{546\text{ nm}} - \Delta A_{573\text{ nm}}) \times \frac{573-554}{573-546}$$

$$\text{cyt } b = \Delta A_{563\text{ nm}} - \Delta A_{573\text{ nm}} - (\Delta A_{546\text{ nm}} - \Delta A_{573\text{ nm}}) \times \frac{573-563}{573-546}$$

Kinetics data from three independent batches of algae were averaged, error bars correspond to standard deviation, and fitted to a first-order kinetics phase (solid line) with an envelope corresponding to the 95% confidence interval (dotted lines) calculated using GraphPad Prism. It means that if 100 batches of algae were grown and measured, 95 kinetics would statistically be contained in this envelope.

Protein isolation and Immunoblot Analysis

For protein accumulation analysis, cells from cultures at 2-4.10^6 cells.ml^{-1} were spun down and were lysed in 50mM Tris pH 6.8, 2% SDS and 1X protease inhibitor (P9599, Sigma-Aldrich) at 37 °C for 30 min. Polypeptides were separated on 4-12 % and 12 % denaturing NuPAGE gels with MOPS running buffer. Antisera raised against cytochrome b_6, PETO, β subunit of ATPsynthase AtpB and STT7 kinase as well as anti-phosphothreonine antibodies (Cell Signaling) were used for immunodetection by ECL.

TMBZ peroxidase activity staining

After polypeptides separation on a 4-12 % NuPAGE gel, heme peroxidase activity was detected by TMBZ (3,3′,5,5′-Tetramethylbenzidine) staining [43]. The gel was incubated for 1 h in the dark in 6.3 mM TMBZ, 175 mM sodium acetate, 30 % methanol, pH 5 before addition of 30 mM H_2O_2. Staining took place at 4 °C in the dark over 72 h. Excess of dye was washed in 175 mM sodium acetate, 30 % isopropanol, pH 5.

Induction of State 1 and State 2

Cells in exponential phase (2-3.10^6 cells.ml^{-1}) in photoheterotrophic conditions in low light (10 $\mu mol_{photons}$ m^{-2} s^{-1}) were concentrated in fresh TAP medium at 2.10^7cells.ml^{-1}. After 1 h recovery in low light, oxidizing conditions induced State 1 (1 h incubation in air, in the light and with 10 µM DCMU). After this pretreatment, State 2 was induced by reducing conditions such as addition of 5 µM membrane uncoupler FCCP (carbonyl cyanide 4-(trifluoromethoxy)phenylhydrazone) in the dark or anaerobic treatment (N_2 flushing on plates) in the dark. FCCP has an effect contrary to the Pasteur effect in yeast (oxygen and ATP production by respiration decreases the rate of glycolysis, this is due to allosteric inhibition of

ATP on phosphofructokinase). In uncoupled cells, ATP levels decrease, the glycolytic flux is upregulated and production of NADPH reduces the plastoquinone pool *via* the NADPH-dehydrogenase, outcompeting the Plastid Terminal Oxidase (for a table reviewing the effects of inhibitor treatments on the PQ pool, see [44]).

State transition was monitored using 77 K fluorescence emission spectra. Chlorophyll was excited with a 455 nm LED and fluorescence was selected with a red-colored filter (high-pass > 600 nm, Kodak Wratten 29 gelatin filter) and measured with an Ocean Optics USB2000 CCD spectrometer. *Chlamydomonas reinhardtii* cells were kept frozen at 77 K in liquid nitrogen during measurement.

PhosTag-PAGE analysis of phosphorylated forms of STT7

To analyze fast and sensitive change of phosphorylation of STT7 kinase, cell cultures were quenched in -20°C acetone at a ratio of 1:4. Precipitated proteins were resuspended in 50 mM Tris pH 6.8, 2 % SDS and desalted using ZebaSpin 7K desalting column (ThermoScientific). Separation of phosphorylated forms was done using Zn-PhosTag (Wako) at 55 µM in Tris-Acetate polyacrylamide gel [45]. Acrylamide:bis-acrylamide ratio in the resolving part of the gels was 75:1. Proteins were transferred during 16 h in a wet blotting apparatus on 0.45 µm nitrocellulose membrane. Immunoblotting was performed with STT7 antisera and ECL detection.

Phosphoproteomics analysis

Purified STT7 kinase domain and WT cyt b_6f complexes were purified and reconstituted *in vitro* with ATP and polypeptides separated on SDS PAGE [10]. STT7 bands were cut out, digested by Trypsin, and sent for phosphoproteomics analysis by tandem CID (collision-induced dissociation) analysis on a Q Exactive (Thermoscientific) to determine phosphorylation sites. The One-to-One threading tool of the Protein Homology/analogY Recognition Engine V 2.0 (PHYRE2 [46]) was used to model the structure of the kinase domain of STT7 based on the crystal structure of the kinase domain of its homolog in Micromonas sp. RCC299 [47].

Acknowledgments

This work was supported by Centre National de la Recherche Scientifique and by the Agence Nationale de la Recherche grant PhotoRegul (ANR-18-CE20-0010-01) and HemeMotion (ANR-22-CE20-0042-01). Daniel Picot is warmly acknowledged for discussions and critical reading of the manuscript. We express our gratitude to Marion Hamon for proteomics analysis.

References

1. Allen, J. F., Bennett, J., Steinback, K. E. & Arntzen, C. J. Chloroplast protein phosphorylation couples plastoquinone redox state to distribution of excitation energy between photosystems. *Nature* **291**, 25–29 (1981).
2. Depège, N., Bellafiore, S. & Rochaix, J.-D. Role of Chloroplast Protein Kinase Stt7 in LHCII Phosphorylation and State Transition in Chlamydomonas. *Science* (2003).
3. Cariti, F. *et al.* Regulation of Light Harvesting in Chlamydomonas reinhardtii Two Protein Phosphatases Are Involved in State Transitions. *Plant Physiol.* **183**, 1749–1764 (2020).
4. Lemaire, C., Girard-Bascou, J., Wollman, F.-A. & Bennoun, P. Studies on the cytochrome b6/f complex. I. Characterization of the complex subunits in Chlamydomonas reinhardtii. *Biochim. Biophys. Acta BBA - Bioenerg.* **851**, 229–238 (1986).
5. Vener, A. V., Van Kan, P. J., Gal, A., Andersson, B. & Ohad, I. Activation/deactivation cycle of redox-controlled thylakoid protein phosphorylation. Role of plastoquinol bound to the reduced cytochrome bf complex. *J. Biol. Chem.* **270**, 25225–25232 (1995).
6. Zito, F. *et al.* The Qo site of cytochrome b6f complexes controls the activation of the LHCII kinase. *EMBO J.* **18**, 2961–2969 (1999).
7. Finazzi, G., Zito, F., Barbagallo, R. P. & Wollman, F. A. Contrasted effects of inhibitors of cytochrome b6f complex on state transitions in Chlamydomonas reinhardtii: the role of Qo site occupancy in LHCII kinase activation. *J. Biol. Chem.* **276**, 9770–9774 (2001).
8. Lemeille, S. *et al.* Analysis of the Chloroplast Protein Kinase Stt7 during State Transitions. *PLoS Biol.* **7**, e45 (2009).
9. Shapiguzov, A. *et al.* Activation of the Stt7/STN7 Kinase through Dynamic Interactions with the Cytochrome b6f Complex. *Plant Physiol.* **171**, 82–92 (2016).
10. Dumas, L. *et al.* A stromal region of cytochrome b6f subunit IV is involved in the activation of the Stt7 kinase in Chlamydomonas. *Proc. Natl. Acad. Sci.* **114**, 12063–12068 (2017).

11. Stroebel, D., Choquet, Y., Popot, J.-L. & Picot, D. An atypical haem in the cytochrome b(6)f complex. *Nature* **426**, 413–418 (2003).
12. Malnoë, A., Wang, F., Girard-Bascou, J., Wollman, F.-A. & de Vitry, C. Thylakoid FtsH protease contributes to photosystem II and cytochrome b6f remodeling in Chlamydomonas reinhardtii under stress conditions. *Plant Cell* **26**, 373–390 (2014).
13. Kuras, R. & Wollman, F. A. The assembly of cytochrome b6/f complexes: an approach using genetic transformation of the green alga Chlamydomonas reinhardtii. *EMBO J.* **13**, 1019–1027 (1994).
14. Kuras, R. *et al.* Molecular genetic identification of a pathway for heme binding to cytochrome b6. *J. Biol. Chem.* **272**, 32427–32435 (1997).
15. Bergner, S. V. *et al.* STATE TRANSITION7-Dependent Phosphorylation Is Modulated by Changing Environmental Conditions, and Its Absence Triggers Remodeling of Photosynthetic Protein Complexes1. *Plant Physiol.* **168**, 615–634 (2015).
16. Hamel, P., Olive, J., Pierre, Y., Wollman, F. A. & de Vitry, C. A new subunit of cytochrome b6f complex undergoes reversible phosphorylation upon state transition. *J. Biol. Chem.* **275**, 17072–17079 (2000).
17. Buchert, F. *et al.* The labile interactions of cyclic electron flow effector proteins. *J. Biol. Chem.* jbc.RA118.004475 (2018) doi:10.1074/jbc.RA118.004475.
18. Chen, X., Kindle, K. & Stern, D. Initiation codon mutations in the Chlamydomonas chloroplast petD gene result in temperature-sensitive photosynthetic growth. *EMBO J.* **12**, 3627–3635 (1993).
19. Zito, F., Vinh, J., Popot, J.-L. & Finazzi, G. Chimeric Fusions of Subunit IV and PetL in the b6 f Complex of Chlamydomonas reinhardtii: STRUCTURAL IMPLICATIONS AND CONSEQUENCES ON STATE TRANSITIONS*. *J. Biol. Chem.* **277**, 12446–12455 (2002).

20. Lemeille, S., Turkina, M. V., Vener, A. V. & Rochaix, J.-D. Stt7-dependent phosphorylation during state transitions in the green alga Chlamydomonas reinhardtii. *Mol. Cell. Proteomics MCP* **9**, 1281–1295 (2010).
21. Delepelaire, P. & Wollman, F.-A. Correlations between fluorescence and phosphorylation changes in thylakoid membranes of *Chlamydomonas reinhardtii* in vivo: A kinetic analysis. *Biochim. Biophys. Acta BBA - Bioenerg.* **809**, 277–283 (1985).
22. Schütz, M. *et al.* Early Evolution of Cytochrome bc Complexes. *J. Mol. Biol.* **300**, 663–675 (2000).
23. Kuras, R., Saint-Marcoux, D., Wollman, F.-A. & de Vitry, C. A specific c-type cytochrome maturation system is required for oxygenic photosynthesis. *Proc. Natl. Acad. Sci.* **104**, 9906–9910 (2007).
24. Saint-Marcoux, D., Wollman, F.-A. & de Vitry, C. Biogenesis of cytochrome b6 in photosynthetic membranes. *J. Cell Biol.* **185**, 1195–1207 (2009).
25. Malnoë, A., Wollman, F.-A., de Vitry, C. & Rappaport, F. Photosynthetic growth despite a broken Q-cycle. *Nat. Commun.* **2**, 301 (2011).
26. de Lacroix de Lavalette, A., Barucq, L., Alric, J., Rappaport, F. & Zito, F. Is the redox state of the ci heme of the cytochrome b6f complex dependent on the occupation and structure of the Qi site and vice versa? *J. Biol. Chem.* **284**, 20822–20829 (2009).
27. Zito, F. & Alric, J. Heme ci or cn of the Cytochrome b6f Complex, A Short Retrospective. in *Cytochrome Complexes: Evolution, Structures, Energy Transduction, and Signaling* (eds. Cramer, W. A. & Kallas, T.) 295–306 (Springer Netherlands, Dordrecht, 2016). doi:10.1007/978-94-017-7481-9_15.
28. Takahashi, H. *et al.* PETO Interacts with Other Effectors of Cyclic Electron Flow in Chlamydomonas. *Mol. Plant* **9**, 558–568 (2016).

29. Proctor, M. S. *et al.* Cryo-EM structures of the Synechocystis sp. PCC 6803 cytochrome b6f complex with and without the regulatory PetP subunit. *Biochem. J.* **479**, 1487–1503 (2022).
30. Rexroth, S. *et al.* Functional Characterization of the Small Regulatory Subunit PetP from the Cytochrome b6f Complex in Thermosynechococcus elongatus. *Plant Cell* **26**, 3435–3448 (2014).
31. Sarewicz, M. *et al.* High-resolution cryo-EM structures of plant cytochrome b6f at work. *Sci. Adv.* **9**, eadd9688 (2023).
32. Perutz, M. F. Stereochemistry of Cooperative Effects in Haemoglobin: Haem–Haem Interaction and the Problem of Allostery. *Nature* **228**, 726–734 (1970).
33. Alric, J., Pierre, Y., Picot, D., Lavergne, J. & Rappaport, F. Spectral and redox characterization of the heme ci of the cytochrome b6f complex. *Proc. Natl. Acad. Sci.* **102**, 15860–15865 (2005).
34. Baymann, F., Giusti, F., Picot, D. & Nitschke, W. The ci/bH moiety in the b6f complex studied by EPR: a pair of strongly interacting hemes. *Proc. Natl. Acad. Sci. U. S. A.* **104**, 519–524 (2007).
35. Yamashita, E., Zhang, H. & Cramer, W. A. Structure of the Cytochrome b6f Complex: Quinone Analogue Inhibitors as Ligands of Heme cn. *J. Mol. Biol.* **370**, 39–52 (2007).
36. Malone, L. A. *et al.* Cryo-EM structure of the spinach cytochrome b6 f complex at 3.6 Å resolution. *Nature* **575**, 535–539 (2019).
37. Gallaher, S. D., Fitz-Gibbon, S. T., Glaesener, A. G., Pellegrini, M. & Merchant, S. S. Chlamydomonas Genome Resource for Laboratory Strains Reveals a Mosaic of Sequence Variation, Identifies True Strain Histories, and Enables Strain-Specific Studies. *Plant Cell* **27**, 2335–2352 (2015).

585 38. Goldschmidt-Clermont, M. Transgenic expression of aminoglycoside adenine transferase
586 in the chloroplast: a selectable marker of site-directed transformation of chlamydomonas.
587 *Nucleic Acids Res.* **19**, 4083–4089 (1991).
588 39. Johnson, X. *et al.* A new setup for in vivo fluorescence imaging of photosynthetic activity.
589 *Photosynth. Res.* **102**, 85–93 (2009).
590 40. Mathiot, C. & Alric, J. Standard units for ElectroChromic Shift measurements in plant
591 biology. *J. Exp. Bot.* **72**, 6467–6473 (2021).
592 41. Joliot, P. & Joliot, A. The low-potential electron-transfer chain in the cytochrome bf
593 complex. *Biochim. Biophys. Acta BBA - Bioenerg.* **933**, 319–333 (1988).
594 42. Joliot, P. & Joliot, A. Electrogenic events associated with electron and proton transfers
595 within the cytochrome b(6)/f complex. *Biochim. Biophys. Acta* **1503**, 369–376 (2001).
596 43. Thomas, P. E., Ryan, D. & Levin, W. An improved staining procedure for the detection of
597 the peroxidase activity of cytochrome P-450 on sodium dodecyl sulfate polyacrylamide
598 gels. *Anal. Biochem.* **75**, 168–176 (1976).
599 44. Alric, J. Cyclic electron flow around photosystem I in unicellular green algae. *Photosynth.*
600 *Res.* **106**, 47–56 (2010).
601 45. Cubillos-Rojas, M. *et al.* Tris-acetate polyacrylamide gradient gels for the simultaneous
602 electrophoretic analysis of proteins of very high and low molecular mass. *Methods Mol.*
603 *Biol. Clifton NJ* **869**, 205–213 (2012).
604 46. Kelley, L. A., Mezulis, S., Yates, C. M., Wass, M. N. & Sternberg, M. J. E. The Phyre2
605 web portal for protein modeling, prediction and analysis. *Nat. Protoc.* **10**, 845–858 (2015).
606 47. Guo, J. *et al.* Structure of the catalytic domain of a state transition kinase homolog from
607 Micromonas algae. *Protein Cell* **4**, 607–619 (2013).

48. Bergner, S. V. *et al.* STATE TRANSITION7-Dependent Phosphorylation Is Modulated by Changing Environmental Conditions, and Its Absence Triggers Remodeling of Photosynthetic Protein Complexes1. *Plant Physiol.* **168**, 615–634 (2015).

Table 1. List of mutant strains used in this work, showing the presence (+) or absence (−) of FTSH protease activity, cyt b_6 and PETO subunits. Most of these strains are impaired for State Transitions (STT).

Strain	Gene	Description	FTSH	Cyt b_6	PETO	STT	Reference
stt7-1	*STT7*	Absence of STT7 mRNA and protein	+	+	+	−	[2]
stt7-9	*STT7*	Insertion of Arg7 at *STT7* 3' end	+	+	+	−	[2,48]
ΔpetB	*petB*	Gene knock-out	+	−	−	−	[13]
iniD1-4	*petA*	Mutation of cyt *f* initiation codon	+	Low	Low	+	[18]
DLSΔ^{suIV}	*petD*	suIV-PetL protein fusion	+	+	Low	Slow	[19]
PWYE^{suIV}	*petD*	Site-directed mutation of PEWY Q_o binding site	+	+	+	−	[6]
R125E^{suIV}	*petD*	suIV Arg125 replaced by Glu	+	+	Low	−	[10]
R207K	*petB*	Fails to accumulate cyt b_6f complex	+	−	n.d.	−	this work
xL215	*petB*	Fails to accumulate cyt b_6f complex	+	−	n.d.	−	this work
G216	*petB*	Fails to accumulate cyt b_6f complex	+	−	n.d.	−	this work
ftsh	*FTSH1*	*ftsh1-1* transformation control WT cyt b_6	−	+	+	Slow	this work
R207K^{b_6}	*petB*	Cyt b_6 Arg207 replaced by Lys	−	+	+	Slower	this work
xL215^{b_6}	*petB*	Cyt b_6 truncated C-terminus	−	+	+	−	this work
G216^{b_6}	*petB*	Cyt b_6 C-terminus elongated with Gly	−	+	+	−	this work

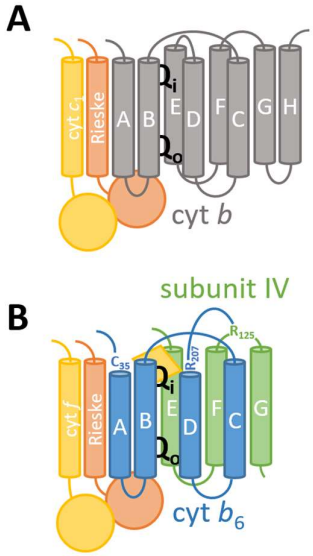

Figure 1. Comparison between (A) the mitochondrial cytochrome bc_1 complex monomer and (B) the chloroplast cyt b_6f complex monomer. In the latter, the cyt *b* is split into cyt b_6 and subunit IV, helix H is missing, $C35^{b6}$ binds heme c_i (yellow diamond) and helix D is not connected to E but to the inter helix F and G loop $R125^{suIV}$. Cyt b_6f also contains a β-carotene and a chlorophyll a molecule (not drawn).

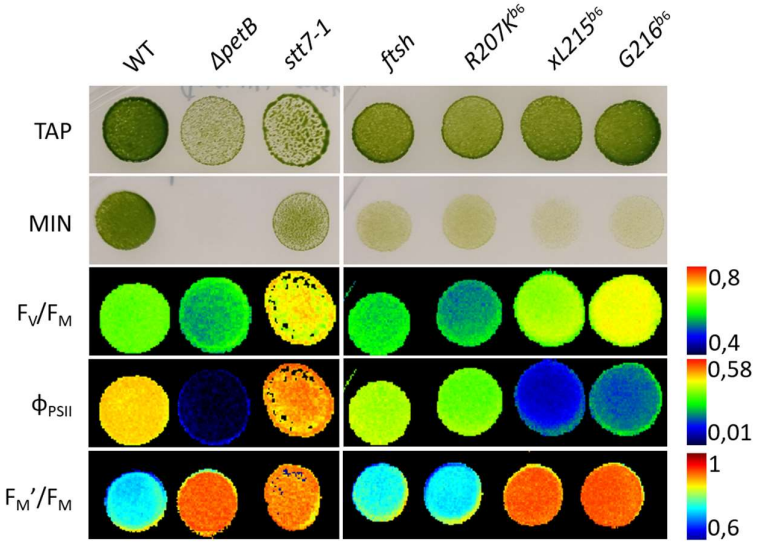

Figure 2. Mutant strains generated for this study and physiological characterization of their photosynthetic properties: heterotrophic growth on tris-acetate-phosphate (TAP, at 5-10 $\mu mol_{photons}\ m^{-2}\ s^{-1}$) and photoautotrophic growth on minimal media (MIN, at 20 $\mu mol_{photons}\ m^{-2}\ s^{-1}$). Fluorescence imaging of TAP-grown cells showed the maximum quantum efficiency of PSII $F_V/F_M = (F_M-F_0) / F_M$, quantum efficiency of PSII in the light $\phi_{PSII} = (F_M'-F) / F_M$ were measured under aerobic conditions using a Chl a fluorescence imaging camera. Fluorescence changes induced by state transitions F_M'/ F_M were measured on aerobic F_M compared to F_M' quenched after 30 minutes of dark anaerobic adaptation (N_2 flushed on the plates). For numerical values, on the false color images see color bars on the right. For the whole kinetics of dark anaerobic adaptation extracted from the time-resolved imaging fluorimeter, see Supplementary Figure S3.

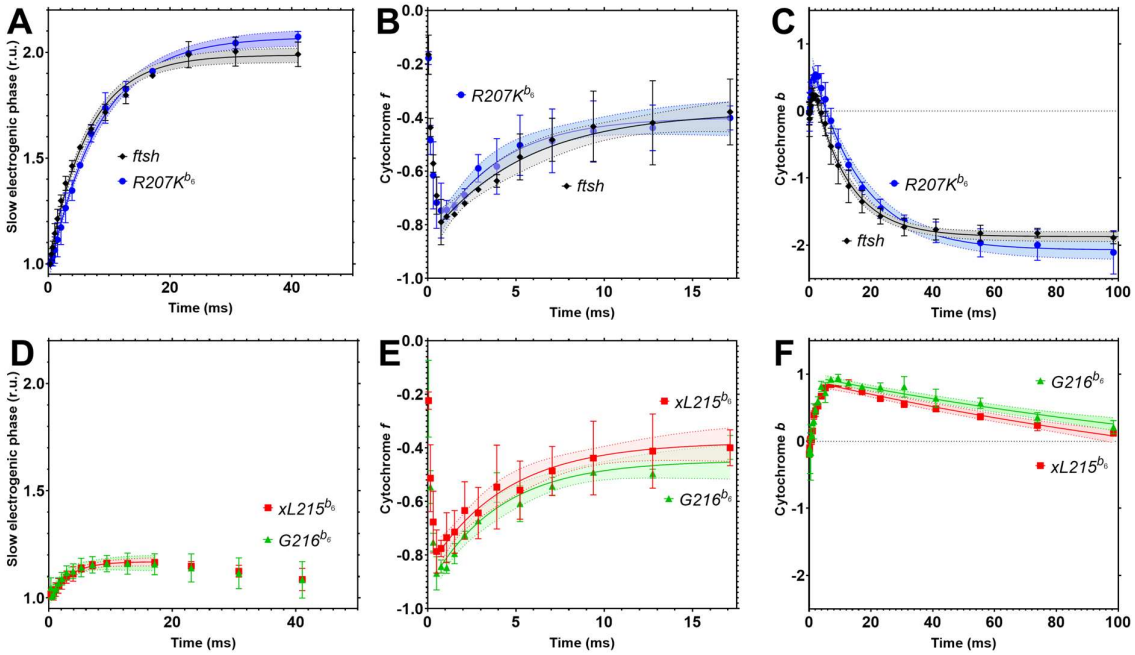

Figure 3. Kinetics of electron transfer in modified cyt b_6f complexes, monitored in anaerobic intact cells treated with 10 µM DCMU and 1 mM hydroxylamine, using flash-induced absorbance changes. (A, D) Electrogenic phase (electrochromic shift at 520 nm) showing the Q_oH_2 to Q_i electron transfer (Q-cycle), through the "low-potential chain" of cofactors b_L, b_H, and c_i. While this phase is not affected in *R207K*^{b_6}, it is strongly reduced in *xL215*^{b_6} and *G216*^{b_6} mutants. (B, E) Cytochrome *f* oxidation by plastocyanin (fast absorbance decrease at 554 nm) and reduction (slower increase) by Q_o shows that the "high-potential chain" is not affected. (C, F) Cytochrome b_L reduction by Q_o, (fast absorbance increase at 563 nm) and oxidation of b_L and b_H (slower decrease) leading to a net oxidation of b_H (reduced in the dark prior to the flash under anoxia) in *R207K*^{b_6}. In *xL215*^{b_6} and *G216*^{b_6} while cyt *b* reduction from Q_o is unchanged, cyt *b* oxidation by Q_i is drastically slowed down due to the absence of heme c_i. Data were fitted on first order kinetics (solid lines) with envelopes corresponding to 95%-confidence intervals.

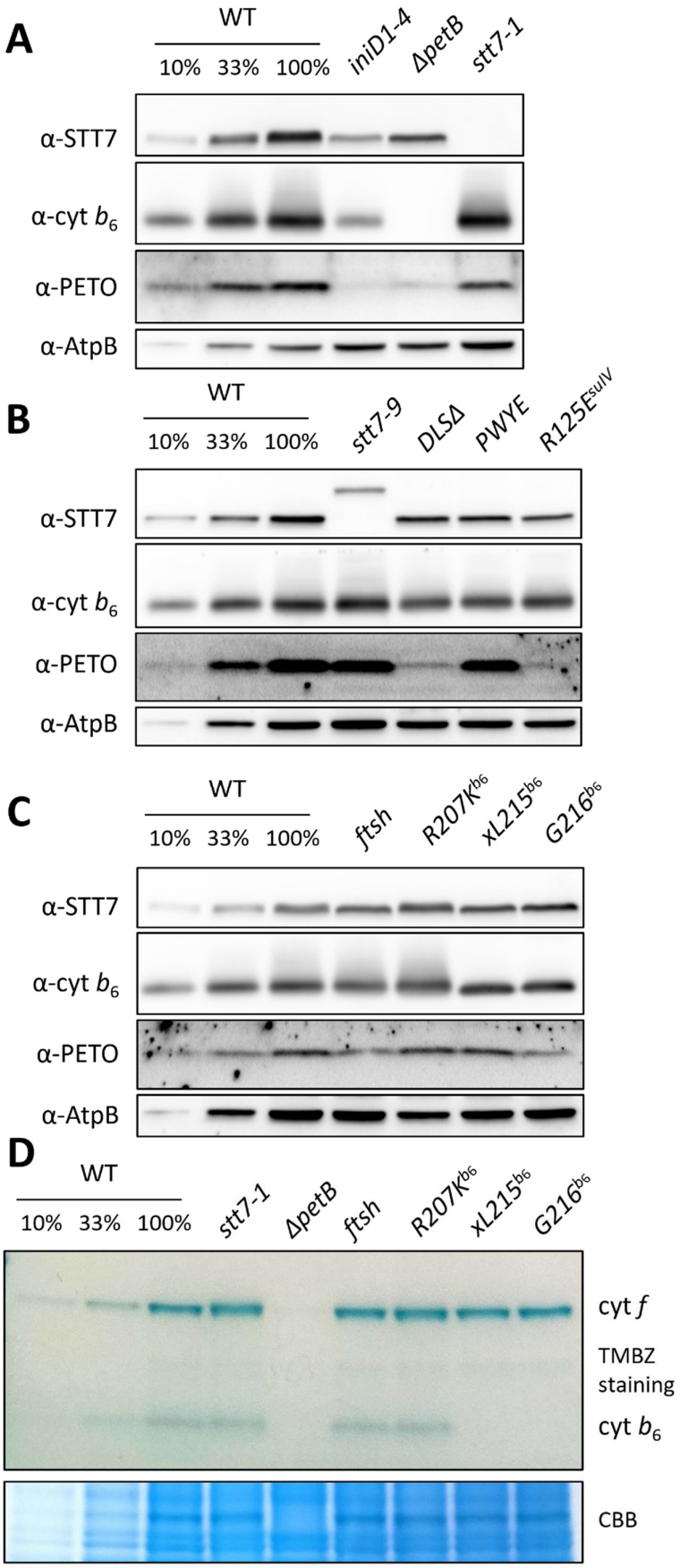
A
WT
10%
33%
100%
iniD1-4
ΔpetB
stt7-1
α-STT7
α-cyt b6
α-PETO
α-AtpB
B
WT
10%
33%
100%
stt7-9
DLSΔ
PWYE
R125E^sulV
α-STT7
α-cyt b6
α-PETO
α-AtpB
C
WT
10%
33%
100%
ftsh
R207K^b6
xL215^b6
G216^b6
α-STT7
α-cyt b6
α-PETO
α-AtpB
D
WT
10%
33%
100%
stt7-1
ΔpetB
ftsh
R207K^b6
xL215^b6
G216^b6
cyt f
TMBZ staining
cyt b6
CBB

651

Figure 4. Accumulation of protein subunits in various control strains and mutants affected for state transitions. Polypeptides, isolated from heterotrophically grown cells, were separated by SDS-PAGE and detected with specific antibodies raised against STT7, cytochrome b_6 and PETO. AtpB was used as loading control (see panels A, B and C). Strain *iniD1-4* accumulates reduced amounts of cyt b_6f complex and the knock-out mutant *ΔpetB* is completely devoid of the complex. The *stt7-1* mutant is devoid of the STT7 protein kinase while in *stt7-9* a different genetic lesion produces smaller amounts of a higher molecular mass of STT7. *PWYE* and *R125E*^{suIV} are site-directed mutants of *petD*, *DLSΔ* is *petD* fused with *petL*. The reference strain *ftsh* is a transformant of *ftsh1-1* with a plasmid carrying non-mutated *petB* while *R207K*^{b6}, *xL215*^{b6} and *G216*^{b6} are *petB* mutants. Panel D shows a gel with heme staining (TMBZ peroxidase activity). Cyt *f* and cyt b_6 do not accumulate in *ΔpetB*. While cyt b_6 subunit is present (panel C), *xL215*^{b6} and *G216*^{b6} show an absence of heme staining of this polypeptide (absence of heme c_i). Cyt *f* staining is equal to WT. Coomassie blue colloidal staining was used as loading control.

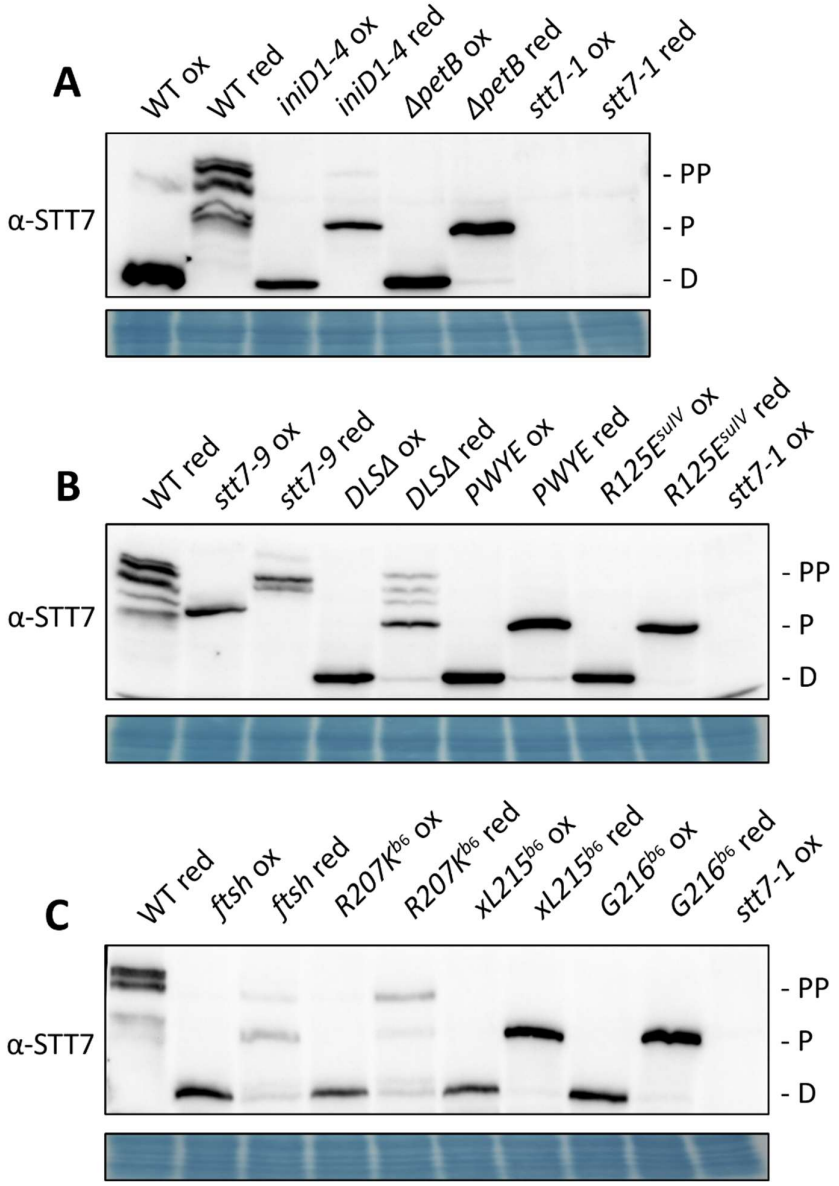

Figure 5. Dynamic changes in STT7 phosphorylation revealed by Phos-tag SDS-PAGE. Phos-tag delays the migration of the phosphorylated forms of polypeptides. Prior to the experiment, oxidizing conditions (ox-label) correspond to a 60 min preillumination in the presence of DCMU (State 1 in the WT). Incubation with 5µM FCCP for 10 min induces the dark reduction (red-label) of the PQ pool (State 2 in the WT). STT7 was detected with a specific antibody. While in all oxidizing conditions (ox), STT7 is mostly dephosphorylated (-D), reducing conditions induced a variety of phosphorylated-forms, -P and -PP, accumulated to various levels. Striking differences are observed between mutant strains. When transferred to reducing conditions, all mutants blocked in State 1 accumulate STT7 under its P-form.

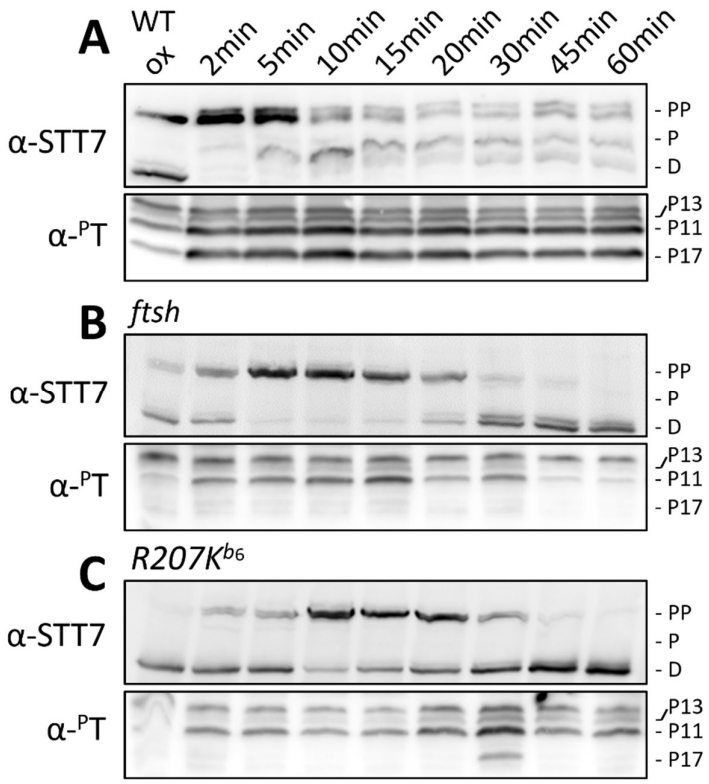

Figure 6. Phosphorylation kinetics of thylakoid polypeptides induced by the reduction of the PQ pool in WT (A), *ftsh* (B) and *R207K*^{b6} (C). Prior to the experiment, oxidizing conditions (ox) correspond to a 60 min preillumination in the presence of DCMU. At $t = 0$, the sample was placed in the dark and FCCP was added. Time resolution is limited to 2 min due to protein extraction. Phosphorylation of STT7 was detected with a specific antibody after Tris-acetate Phos-tag SDS-PAGE. Various forms of STT7 were detected: dephosphorylated (-D), mildly phosphorylated (-P) and highly phosphorylated (-PP). Phosphorylation of light harvesting complexes polypeptides was detected after Bis-Tris SDS-PAGE using an anti phosphothreonine antibody (α-^{P}T). Phosphorylation of polypeptides P13 and P17 are specific for State 2.

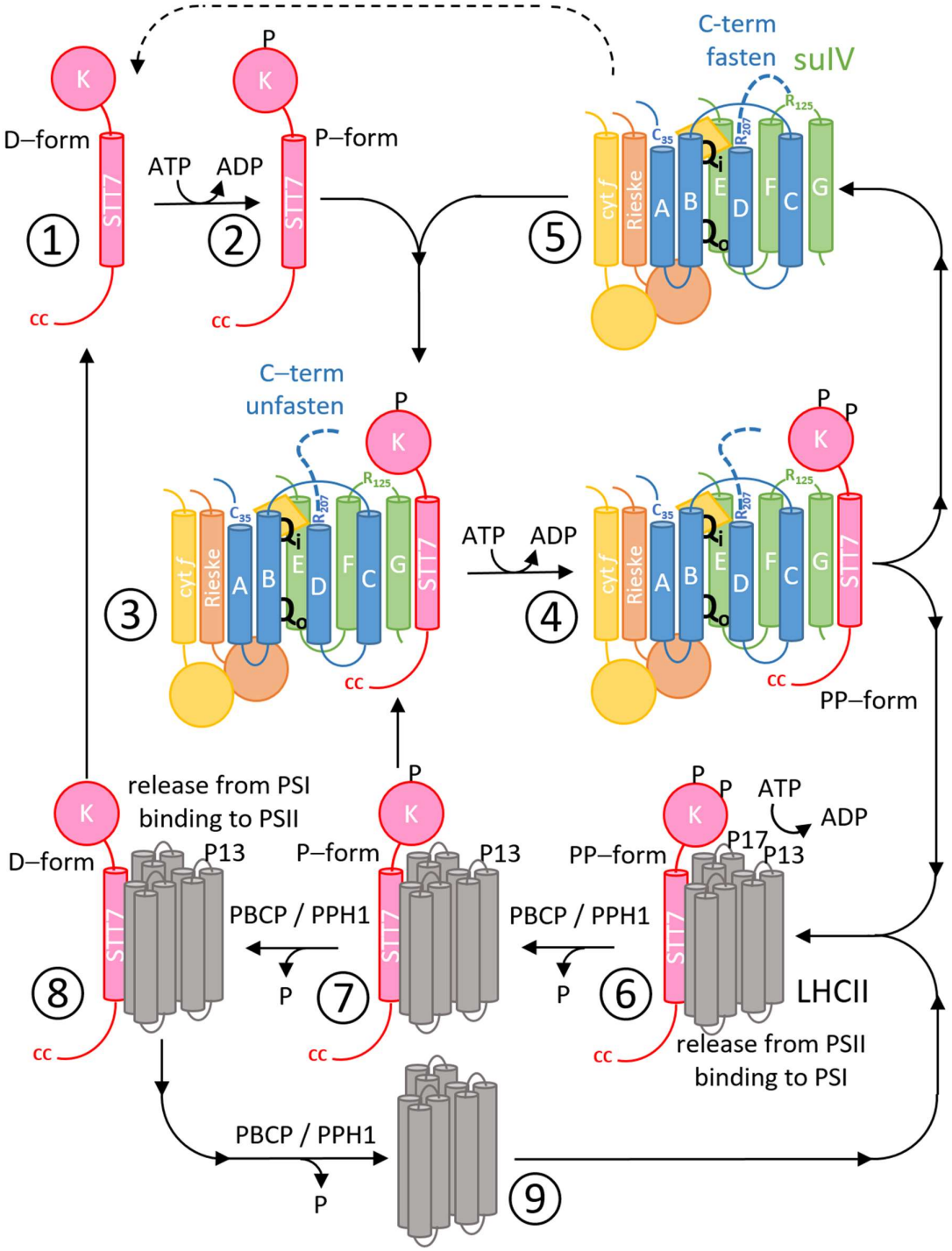

Figure 7. Model for cyt b_6f complex – STT7 protein kinase interaction, phosphorylations and state transitions (see text for details). The first phosphorylation step ① to ② is independent from cyt b_6f complex (see Δ*petB* in Figure 4A). STT7 binds to the F-G interface of subunit IV and interacts directly with $R125^{sulV}$, steps ⑤ to ③. The cytochrome is required for the formation of the highly phosphorylated form of STT7, step ③ to ④ and the phosphorylation of P13 and P17 of light harvesting complexes II. PBCP and PPH1 phosphatases dephosphorylate LHCII, steps ⑥ to ⑨.

Supplementary Information

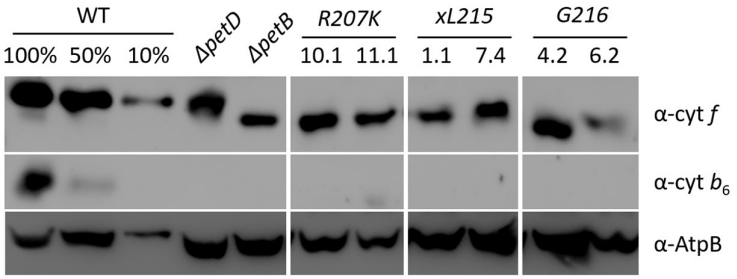

Figure S1. Unsuccessful attempts to obtain modified cyt b_6 when FTSH is active. Transformants of a *ΔPetB* strain were sequenced to verify the presence of the mutated *PetB* genes, but none of these mutants accumulated the cyt b_6 subunit neither did they grow under photoautotrophic conditions.

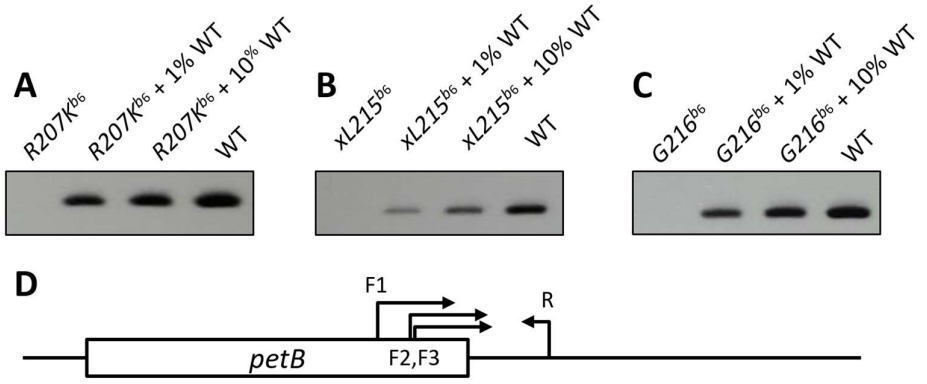

Figure S2. Genetic transformation of *ftsh 1-1* strain provided homoplasmic site directed mutants of the chloroplast *petB* gene. This is shown by WT-specific PCR on DNA extracts of mutants $R207K^{b6}$ (A) $xL215^{b6}$ (B) and $G216^{b6}$ (C). 10% and 1% dilutions of WT DNA extract were added to the mutant DNA extract to probe the sensitivity of the PCR. PCR primers used were (same reverse R for A, B and C) TTATCAATGGGCCAACGGGG and ATGTTAATGCACTTCTTAATGATTCGT (forward-specific F1, see A), CGTAAACAAGGTATTTCAGGTCCTCTA (F2, see B), AAACAAGGTATTTCAGGTCCTCTATAA (F3, see C), see (D) for illustration.

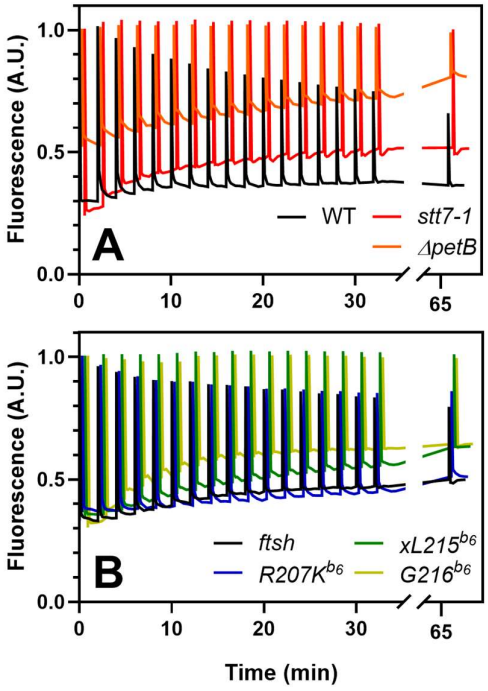

Figure S3. Kinetics of chlorophyll fluorescence quenching upon dark anaerobic adaptation (State 1 to State 2 transition). These data are from the same dataset as in Figure 2 from the main text. Anoxia was induced at $t = 0$ by flushing N_2 onto the plate. Saturating pulses were used to probe F_M'. The rise of the steady-state fluorescence F' is induced by the non-photochemical reduction of the PQ pool (reductive redox poise in anoxic cells). (A) The WT strain shows a quenching of F_M' absent from mutants blocked for state transitions (*stt7-1* and *ΔpetB*). (B) While *ftsh* and *R207K*^{b_6} are similar to the WT, *xL215*^{b_6} and *G216*^{b_6} are close to *stt7-1*.

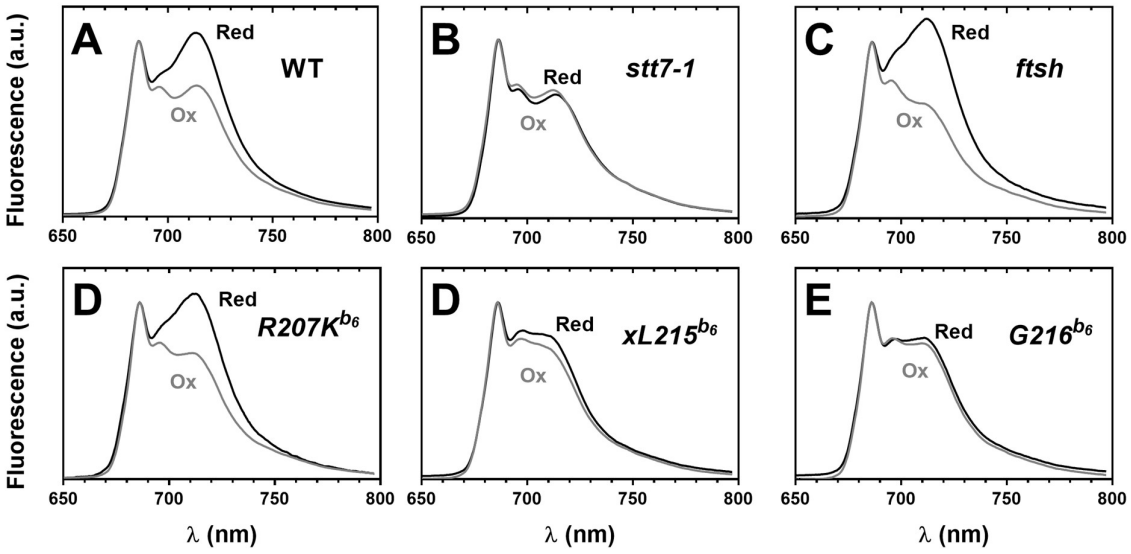

Figure S4. State transitions measured as 77K chlorophyll fluorescence emission spectra. Spectra in oxidizing (Ox) and reducing (Red) conditions were normalized on the PSII emission peak at 685 nm. While WT, *ftsh* and *R207K*^{b_6} show an increased PSI emission at 715 nm in reducing conditions, the *stt7-1*, *xL215*^{b_6} and *G216*^{b_6} mutants did not.

References

1. Allen, J. F., Bennett, J., Steinback, K. E. & Arntzen, C. J. Chloroplast protein phosphorylation couples plastoquinone redox state to distribution of excitation energy between photosystems. *Nature* **291**, 25–29 (1981).
2. Depège, N., Bellafiore, S. & Rochaix, J.-D. Role of Chloroplast Protein Kinase Stt7 in LHCII Phosphorylation and State Transition in Chlamydomonas. *Science* (2003).
3. Cariti, F. *et al.* Regulation of Light Harvesting in Chlamydomonas reinhardtii Two Protein Phosphatases Are Involved in State Transitions. *Plant Physiol.* **183**, 1749–1764 (2020).
4. Lemaire, C., Girard-Bascou, J., Wollman, F.-A. & Bennoun, P. Studies on the cytochrome b6/f complex. I. Characterization of the complex subunits in Chlamydomonas reinhardtii. *Biochim. Biophys. Acta BBA - Bioenerg.* **851**, 229–238 (1986).
5. Vener, A. V., Van Kan, P. J., Gal, A., Andersson, B. & Ohad, I. Activation/deactivation cycle of redox-controlled thylakoid protein phosphorylation. Role of plastoquinol bound to the reduced cytochrome bf complex. *J. Biol. Chem.* **270**, 25225–25232 (1995).
6. Zito, F. *et al.* The Qo site of cytochrome b6f complexes controls the activation of the LHCII kinase. *EMBO J.* **18**, 2961–2969 (1999).
7. Finazzi, G., Zito, F., Barbagallo, R. P. & Wollman, F. A. Contrasted effects of inhibitors of cytochrome b6f complex on state transitions in Chlamydomonas reinhardtii: the role of Qo site occupancy in LHCII kinase activation. *J. Biol. Chem.* **276**, 9770–9774 (2001).
8. Lemeille, S. *et al.* Analysis of the Chloroplast Protein Kinase Stt7 during State Transitions. *PLoS Biol.* **7**, e45 (2009).
9. Shapiguzov, A. *et al.* Activation of the Stt7/STN7 Kinase through Dynamic Interactions with the Cytochrome b6f Complex. *Plant Physiol.* **171**, 82–92 (2016).
10. Dumas, L. *et al.* A stromal region of cytochrome b6f subunit IV is involved in the activation of the Stt7 kinase in Chlamydomonas. *Proc. Natl. Acad. Sci.* **114**, 12063–12068 (2017).
11. Stroebel, D., Choquet, Y., Popot, J.-L. & Picot, D. An atypical haem in the cytochrome b(6)f complex. *Nature* **426**, 413–418 (2003).

12. Malnoë, A., Wang, F., Girard-Bascou, J., Wollman, F.-A. & de Vitry, C. Thylakoid FtsH protease contributes to photosystem II and cytochrome b6f remodeling in Chlamydomonas reinhardtii under stress conditions. *Plant Cell* **26**, 373–390 (2014).
13. Kuras, R. & Wollman, F. A. The assembly of cytochrome b6/f complexes: an approach using genetic transformation of the green alga Chlamydomonas reinhardtii. *EMBO J.* **13**, 1019–1027 (1994).
14. Kuras, R. *et al.* Molecular genetic identification of a pathway for heme binding to cytochrome b6. *J. Biol. Chem.* **272**, 32427–32435 (1997).
15. Bergner, S. V. *et al.* STATE TRANSITION7-Dependent Phosphorylation Is Modulated by Changing Environmental Conditions, and Its Absence Triggers Remodeling of Photosynthetic Protein Complexes1. *Plant Physiol.* **168**, 615–634 (2015).
16. Hamel, P., Olive, J., Pierre, Y., Wollman, F. A. & de Vitry, C. A new subunit of cytochrome b6f complex undergoes reversible phosphorylation upon state transition. *J. Biol. Chem.* **275**, 17072–17079 (2000).
17. Buchert, F. *et al.* The labile interactions of cyclic electron flow effector proteins. *J. Biol. Chem.* jbc.RA118.004475 (2018) doi:10.1074/jbc.RA118.004475.
18. Chen, X., Kindle, K. & Stern, D. Initiation codon mutations in the Chlamydomonas chloroplast petD gene result in temperature-sensitive photosynthetic growth. *EMBO J.* **12**, 3627–3635 (1993).
19. Zito, F., Vinh, J., Popot, J.-L. & Finazzi, G. Chimeric Fusions of Subunit IV and PetL in the b6 f Complex of Chlamydomonas reinhardtii: STRUCTURAL IMPLICATIONS AND CONSEQUENCES ON STATE TRANSITIONS*. *J. Biol. Chem.* **277**, 12446–12455 (2002).
20. Lemeille, S., Turkina, M. V., Vener, A. V. & Rochaix, J.-D. Stt7-dependent phosphorylation during state transitions in the green alga Chlamydomonas reinhardtii. *Mol. Cell. Proteomics MCP* **9**, 1281–1295 (2010).
21. Delepelaire, P. & Wollman, F.-A. Correlations between fluorescence and phosphorylation changes in thylakoid membranes of *Chlamydomonas reinhardtii* in vivo: A kinetic analysis. *Biochim. Biophys. Acta BBA - Bioenerg.* **809**, 277–283 (1985).
22. Schütz, M. *et al.* Early Evolution of Cytochrome bc Complexes. *J. Mol. Biol.* **300**, 663–675 (2000).

787 23. Kuras, R., Saint-Marcoux, D., Wollman, F.-A. & de Vitry, C. A specific c-type cytochrome
788 maturation system is required for oxygenic photosynthesis. *Proc. Natl. Acad. Sci.* **104**, 9906–9910
789 (2007).
790 24. Saint-Marcoux, D., Wollman, F.-A. & de Vitry, C. Biogenesis of cytochrome b6 in photosynthetic
791 membranes. *J. Cell Biol.* **185**, 1195–1207 (2009).
792 25. Malnoë, A., Wollman, F.-A., de Vitry, C. & Rappaport, F. Photosynthetic growth despite a broken
793 Q-cycle. *Nat. Commun.* **2**, 301 (2011).
794 26. de Lacroix de Lavalette, A., Barucq, L., Alric, J., Rappaport, F. & Zito, F. Is the redox state of the
795 ci heme of the cytochrome b6f complex dependent on the occupation and structure of the Qi site
796 and vice versa? *J. Biol. Chem.* **284**, 20822–20829 (2009).
797 27. Zito, F. & Alric, J. Heme ci or cn of the Cytochrome b6f Complex, A Short Retrospective. in
798 *Cytochrome Complexes: Evolution, Structures, Energy Transduction, and Signaling* (eds. Cramer,
799 W. A. & Kallas, T.) 295–306 (Springer Netherlands, Dordrecht, 2016). doi:10.1007/978-94-017-
800 7481-9_15.
801 28. Takahashi, H. *et al.* PETO Interacts with Other Effectors of Cyclic Electron Flow in
802 Chlamydomonas. *Mol. Plant* **9**, 558–568 (2016).
803 29. Proctor, M. S. *et al.* Cryo-EM structures of the Synechocystis sp. PCC 6803 cytochrome b6f
804 complex with and without the regulatory PetP subunit. *Biochem. J.* **479**, 1487–1503 (2022).
805 30. Rexroth, S. *et al.* Functional Characterization of the Small Regulatory Subunit PetP from the
806 Cytochrome b6f Complex in Thermosynechococcus elongatus. *Plant Cell* **26**, 3435–3448 (2014).
807 31. Sarewicz, M. *et al.* High-resolution cryo-EM structures of plant cytochrome b6f at work. *Sci. Adv.*
808 **9**, eadd9688 (2023).
809 32. Perutz, M. F. Stereochemistry of Cooperative Effects in Haemoglobin: Haem–Haem Interaction
810 and the Problem of Allostery. *Nature* **228**, 726–734 (1970).
811 33. Alric, J., Pierre, Y., Picot, D., Lavergne, J. & Rappaport, F. Spectral and redox characterization of
812 the heme ci of the cytochrome b6f complex. *Proc. Natl. Acad. Sci.* **102**, 15860–15865 (2005).
813 34. Baymann, F., Giusti, F., Picot, D. & Nitschke, W. The ci/bH moiety in the b6f complex studied by
814 EPR: a pair of strongly interacting hemes. *Proc. Natl. Acad. Sci. U. S. A.* **104**, 519–524 (2007).

35. Yamashita, E., Zhang, H. & Cramer, W. A. Structure of the Cytochrome b6f Complex: Quinone Analogue Inhibitors as Ligands of Heme cn. *J. Mol. Biol.* **370**, 39–52 (2007).
36. Malone, L. A. *et al.* Cryo-EM structure of the spinach cytochrome b6 f complex at 3.6 Å resolution. *Nature* **575**, 535–539 (2019).
37. Gallaher, S. D., Fitz-Gibbon, S. T., Glaesener, A. G., Pellegrini, M. & Merchant, S. S. Chlamydomonas Genome Resource for Laboratory Strains Reveals a Mosaic of Sequence Variation, Identifies True Strain Histories, and Enables Strain-Specific Studies. *Plant Cell* **27**, 2335–2352 (2015).
38. Goldschmidt-Clermont, M. Transgenic expression of aminoglycoside adenine transferase in the chloroplast: a selectable marker of site-directed transformation of chlamydomonas. *Nucleic Acids Res.* **19**, 4083–4089 (1991).
39. Johnson, X. *et al.* A new setup for in vivo fluorescence imaging of photosynthetic activity. *Photosynth. Res.* **102**, 85–93 (2009).
40. Mathiot, C. & Alric, J. Standard units for ElectroChromic Shift measurements in plant biology. *J. Exp. Bot.* **72**, 6467–6473 (2021).
41. Joliot, P. & Joliot, A. The low-potential electron-transfer chain in the cytochrome bf complex. *Biochim. Biophys. Acta BBA - Bioenerg.* **933**, 319–333 (1988).
42. Joliot, P. & Joliot, A. Electrogenic events associated with electron and proton transfers within the cytochrome b(6)/f complex. *Biochim. Biophys. Acta* **1503**, 369–376 (2001).
43. Thomas, P. E., Ryan, D. & Levin, W. An improved staining procedure for the detection of the peroxidase activity of cytochrome P-450 on sodium dodecyl sulfate polyacrylamide gels. *Anal. Biochem.* **75**, 168–176 (1976).
44. Alric, J. Cyclic electron flow around photosystem I in unicellular green algae. *Photosynth. Res.* **106**, 47–56 (2010).
45. Cubillos-Rojas, M. *et al.* Tris-acetate polyacrylamide gradient gels for the simultaneous electrophoretic analysis of proteins of very high and low molecular mass. *Methods Mol. Biol. Clifton NJ* **869**, 205–213 (2012).

842 46. Kelley, L. A., Mezulis, S., Yates, C. M., Wass, M. N. & Sternberg, M. J. E. The Phyre2 web portal
843 for protein modeling, prediction and analysis. *Nat. Protoc.* **10**, 845–858 (2015).
844 47. Guo, J. *et al.* Structure of the catalytic domain of a state transition kinase homolog from Micromonas
845 algae. *Protein Cell* **4**, 607–619 (2013).
846 48. Bergner, S. V. *et al.* STATE TRANSITION7-Dependent Phosphorylation Is Modulated by
847 Changing Environmental Conditions, and Its Absence Triggers Remodeling of Photosynthetic
848 Protein Complexes1. *Plant Physiol.* **168**, 615–634 (2015).
849
850